Industrial Chemistry & Materials

ROYAL SOCIETY OF CHEMISTRY

PAPER

View Article Online
View Journal | View Issue

Cite this: *Ind. Chem. Mater.*, 2026, **4**, 118

Continuous direct air capture and conversion tandem system applicable to a wide range of CO_2 concentrations†

Shinta Miyazaki, [a] Akihiko Anzai, *[a] Masaki Yoshihara,[a] Hsu Sheng Feng,[a] Shinya Mine, [b] Takashi Toyao [a] and Ken-ichi Shimizu *[a]

The concentrations of CO_2 emitted from different CO_2 sources vary significantly. Thus, processes capable of accommodating a broad range of CO_2 concentrations, from 0.04% (air) to 10% (power plants), must be developed to achieve carbon neutrality. In this study, we developed a two-step CO_2 capture and hydrogenation system by employing Rb-oxide-incorporated zeolites as CO_2 adsorbents and Ni/CeO_2 or $Cu/ZnO/Al_2O_3$ as catalysts for CO_2 hydrogenation. This process is suitable for continuous operation over a temperature swing of 40–200 °C. Notably, this system can operate at low temperatures (below 200 °C) using a simple temperature-swing process in the presence of O_2. Compared with more than 100 previously reported systems that can convert CO_2 including O_2 to green fuels such as CO or CH_4, the proposed system achieved the best CO_2 conversions to CH_4 and CO.

Received 21st February 2025,
Accepted 12th June 2025

DOI: 10.1039/d5im00028a

rsc.li/icm

Keywords: Direct air capture (DAC); Zeolite sorbent; Temperature swing adsorption (TSA); Methanation; Reverse water-gas shift (RWGS).

1 Introduction

Anthropogenic greenhouse gas emissions are critical in causing global warming.[1,2] To mitigate global warming and achieve a carbon-neutral society, the amount of CO_2 emitted from energy- and industry-related sources must be significantly reduced.[3,4] One of the most promising strategies for mitigating anthropogenic CO_2 emissions is to convert CO_2 into chemical fuels, such as methane or methanol, and value-added chemicals *via* syngas using green H_2 produced *via* water electrolysis using renewable energy sources such as wind and solar power.[5,6] Large-scale production of green H_2 using water electrolysis has already been initiated at sites such as the Shell Energy and Chemicals Park Rheinland in Germany.[7] These efforts highlight the increasing demand for practical CO_2 capture and utilization (CCU) technologies utilizing green H_2. However, in CCU technologies, CO_2 needs to be captured from emission sources (such as power, refinery, chemical, steel, and ceramic plants) and stored prior to chemical transformation.[8] Although liquid amine scrubbing is a commonly employed CO_2 capture and storage (CCS) technology in industry,[9] it is hindered by high costs, significant energy requirements for solvent regeneration, and the need for large-scale plants.[10]

CO_2 needs to be captured from emission sources (such as power, refinery, chemical, steel, and ceramic plants) and stored prior to chemical transformation.[8] Although liquid amine scrubbing is a commonly employed CO_2 capture and storage (CCS) technology in the industry,[9] it is hindered by high costs, significant energy requirements for solvent regeneration, and the need for large-scale plants.[10]

Recently, unsteady-state CO_2 hydrogenation processes, known as CO_2 capture and reduction (CCR) and integrated CO_2 capture and conversion, have emerged as alternative technologies in which the need for CCS is avoided.[11,12] In 2016, Urakawa *et al.*[13] and Farrauto *et al.*[14] separately published their works on CCR. Unlike conventional methods, CCR does not require large amounts of thermal energy for CO_2 separation and purification.[15] Furthermore, this process is theoretically applicable to the utilization of O_2-containing CO_2 emitted from industries such as power plants and is advantageous for practical use.[16]

Dual-functional materials (DFMs) in which alkali or alkaline earth metals for CO_2 capture are combined with transition metals for CO_2 hydrogenation are widely used in CCR operations. Selective CH_4 and CO formation has been reported in various CCR studies (Table S1†). However, the

[a] *Institute for Catalysis, Hokkaido University, Sapporo, Hokkaido, Japan. E-mail: anzai.akihiko@cat.hokudai.ac.jp, kshimizu@cat.hokudai.ac.jp*
[b] *Research Institute for Chemical Process Technology, National Institute of Advanced Industrial Science and Technology, 4-2-1, Nigatake, Sendai, Miyagino-ku, Miyagi, Japan*

† Electronic supplementary information (ESI) available. See DOI: https://doi.org/10.1039/d5im00028a

reported CCR processes cannot be integrated with effluent streams released from various industrial processes because these are performed by changing the gas conditions stepwise (Fig. 1a). To address this, Urakawa *et al.* proposed a two-reactor parallel-type system for continuous CCR,[13] whereas we developed a two-reactor parallel-type system for the continuous production of green fuels, such as CH_4 [17,18] and CO,[19,20] from a $CO_2 + O_2/N_2$ mixture by alternating the feeds of $CO_2 + O_2/N_2$ and H_2 to the DFMs in the two reactors (Fig. 1b).

Our system can continuously capture low-concentration CO_2 (below 1%) from a mixture of O_2 and convert it into green fuels. However, continuous CCR is not applicable to high-concentration CO_2 emissions that are similar to exhaust gas emissions from thermal power plants and other industrial sources because of the limited CO_2 capacity of DFMs[21] compared with zeolite sorbents.[22,23] For example, less than 30% high-concentration inlet CO_2 (10%) can be converted even when one of the highest-activity DFMs available is used under optimized conditions (Fig. S1 and ESI† Text S1). This is because materials such as CaO—one of the most effective basic metal oxides used in DFMs—store CO_2 *via* a bulk diffusion mechanism, in which CO_2 must pass through $CaCO_3$ crystals to reach the unreacted CaO core.[24] Only surface carbonates are consumed during the reaction, while bulk carbonates remain inaccessible.[25] Consequently, this limitation restricts their applicability to dilute CO_2 streams. To effectively convert both diluted and high-concentration CO_2 (such as from thermal power plants and other industrial sources), it becomes essential to employ materials offering a range of adsorption site strengths and affinities. In contrast to DFMs, CO_2 can also be physically adsorbed onto sorbents like zeolites, enabling CO_2 adsorption and desorption under mild temperature swing conditions.[26,27] However, removing the thermodynamic equilibrium constraint imposed by low temperatures to ensure high CO_2 conversion appears to be an insurmountable dilemma in continuous CCR. Accordingly, our central motivation was to overcome the limitation of CCR and expand the application to a wide range of CO_2 concentrations, from direct air capture (DAC) to flue gas, while maintaining high performance.

In this study, we developed a novel system in which tandem CO_2 capture and hydrogenation are achieved by combining Rb-loaded zeolites (Rb-zeolites) as CO_2 adsorbents with CO_2 hydrogenation catalysts (Fig. 1c, and a detailed explanation of these three unsteady-state CO_2 hydrogenation processes is provided in ESI† Text S2). For CO_2 capture, zeolites were used as typical economically viable solid adsorbents. Unlike liquid and solid amines, zeolites do not produce toxic degradation products.[28] In addition, zeolites show greater stability than metal–organic frameworks (MOFs), which are also well-known solid adsorbents.[29,30] For CO_2 hydrogenation, Ni/CeO_2 [31–33] and $Cu/ZnO/Al_2O_3$ [34–36] were used as typical catalysts for methanation and reverse water-gas shift (RWGS) reactions, respectively. Ni/CeO_2 [37–40] and $Cu/ZnO/Al_2O_3$,[41–44] easily prepared by a simple method, are promising catalysts for the tandem system toward practical implementation. The sorbents were filled upstream in two parallel reactors. The catalyst was filled downstream in a single reactor. The system was based on continuous temperature swing adsorption (TSA) and catalytic reactions. Initially, a $CO_2 + O_2/N_2$ mixture was fed into the Rb-zeolite sorbent (denoted as Z) to capture CO_2 (eqn (1)). After this mixture changed to pure H_2 gas and the sorbent temperature was increased, the captured CO_2 and H_2 were simultaneously desorbed by applying heat (eqn (2)). Desorbed CO_2 and H_2 flowed to the bottom reactor, and the methanation or RWGS reaction proceeded using the catalysts (eqn (3) and (4)).

$$CO_2\ (gas) + Z \rightarrow Z\text{-}CO_2\ (ad) \quad (1)$$

$$H_2 + Z\text{-}CO_2\ (ad) \rightarrow CO_2\ (gas) + H_2\ (gas) + Z \quad (2)$$

$$CO_2\ (gas) + 4H_2\ (gas) \rightarrow CH_4\ (gas) + 2H_2O\ (gas) \quad (3)$$

$$CO_2\ (gas) + H_2\ (gas) \rightarrow CO\ (gas) + H_2O\ (gas) \quad (4)$$

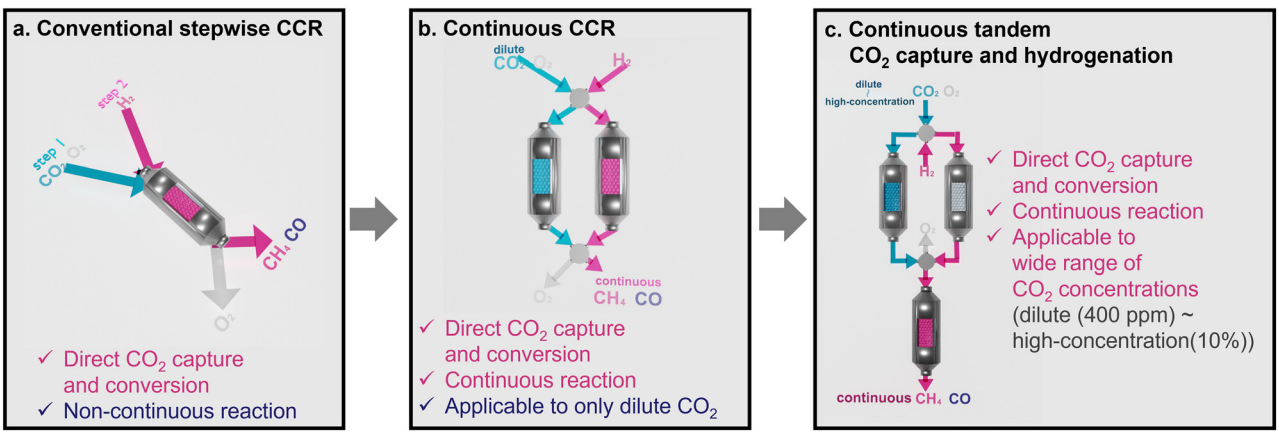

Fig. 1 Conceptual diagram of (a) conventional stepwise CCR, (b) continuous CCR, and (c) continuous tandem CO_2 capture and hydrogenation processes.

This new process is suitable for continuous operation under temperature-swing cycling in the low-temperature range (between 40 and 200 °C) in the presence of O_2. Compared with more than 100 reported CCR processes, this novel process exhibited high inlet CO_2 conversion.

2 Results and discussion

2.1 Screening and optimizing sorbents and catalysts

First, we examined the CO_2 adsorption properties of zeolite sorbents at 50 °C using a fixed-bed continuous-flow system (Fig. S2†). The breakthrough curve obtained from the CO_2 adsorption measurements is shown in Fig. 2a, and the CO_2 adsorption amount determined from the breakthrough curve is presented in Fig. 2b. Among Rb-zeolites (such as Rb-13X, Rb-Y, and Rb-beta) and alkali-metal-loaded beta zeolites (such as Rb-, Na-, K-, and Cs-beta), Rb-beta exhibited the highest amount of CO_2 adsorption. Similarly, we investigated the CO_2 adsorption properties of bare beta zeolite (H-beta) as a reference for comparison with Rb-beta (Fig. S3†). The introduction of Rb^+ cations increased the CO_2 adsorption capacity, suggesting that the framework oxygen atoms became more electron-rich due to the presence of the basic alkali metal cations.[45] This result is consistent with previous reports.[46,47] It is considered that physisorbed CO_2, which interacts weakly with the framework oxygen atoms, was more effectively stabilized within the zeolite structure.

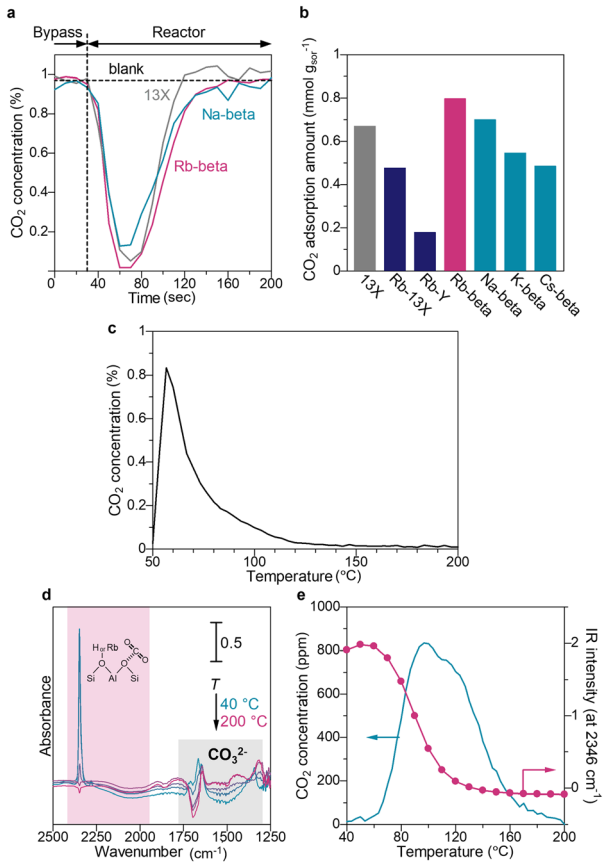

Fig. 2 (a) CO_2 adsorption at 50 °C for 200 s under a flow of 0.97% CO_2 (He balance; total flow: 100 mL min^{-1}). The flow passed through a bypass line in the first 20 s; (b) Comparison between CO_2 adsorption amounts on zeolite sorbents at 50 °C (determined by conducting the experiment shown in Fig. 1a); (c) CO_2 TPD profiles for Rb-beta under He flow. Conditions: heated at 500 °C under He flow and then cooled to 50 °C under He flow; 1% CO_2/N_2 mixture was fed into the reactor at 50 °C for 30 min and purged with He for 5 min. The CO_2 TPD experiment was conducted by applying heat under He flow; (d) *operando* FTIR spectroscopy for Rb-beta under CO_2 TPD condition. IR spectra of adsorbed species at temperature intervals of 40 °C; (e) time-resolved trends in the IR intensities of adsorbed CO_2; concentration of desorbed CO_2. The background spectrum was recorded before CO_2 capture.

Subsequently, we performed temperature-programmed desorption (TPD) measurements of CO_2 to explore the CO_2 desorption properties of Rb-beta (Fig. 2c). CO_2 desorption from Rb-beta was observed over the temperature range of 50–150 °C, and the total amount of desorbed CO_2 (0.8 mmol g^{-1}) was close to the CO_2 adsorption amount (0.8 mmol g^{-1}). This indicated that adsorbed CO_2 at 50 °C was completely desorbed after heating to 150 °C. To investigate zeolite structure, Fig. S4† shows XRD patterns of alkali-metal-loaded beta zeolite samples. XRD peaks of alkali-metal-loaded beta zeolites closely resembled those of H-beta, indicating that the zeolite framework remained intact after immobilizing alkali metals.

To elucidate the mechanism underlying CO_2 adsorption and desorption, *operando* Fourier transform infrared (FTIR) spectroscopy was performed during the TPD of CO_2 on Rb-beta. A schematic of the setup is shown in Fig. S5.† Prior to the experiment, the infrared (IR) disk was heated under He at 400 °C for 30 min and then cooled to 40 °C. To record the background spectrum, 1% CO_2/He was fed to the sample at 40 °C for 5 min and purged under He. A strong band at 2275 cm^{-1} assigned to the physically adsorbed CO_2 on zeolite[48,49] and two weak broad bands at 1720 and 1280 cm^{-1} assigned to the carbonate species[50,51] were observed before heating (Fig. 2d). These results indicated that physically adsorbed CO_2 was the main adsorbed species and carbonate was a minor species. As the temperature increased from 60 to 160 °C, the band intensity for the physically adsorbed CO_2 sharply decreased, accompanied by CO_2 formation at the outlet of the IR cell (Fig. 2e). This indicated that the physical adsorption and desorption of CO_2 were responsible for the adsorption/desorption of CO_2 on Rb-beta.

We adopted Ni/CeO_2 and Cu/ZnO/Al_2O_3 as typical catalysts for the methanation and RWGS reactions. The reaction temperatures for these catalysts were optimized by performing steady-state reaction experiments (Fig. 3). When the Ni/CeO_2 catalyst was used, the CO_2 conversion and CH_4 selectivity sharply increased at a temperature of >150 °C (Fig. 3a). The reaction over the temperature range of 200–500 °C resulted in nearly complete conversion of CO_2 to CH_4 (CO_2 conversion ≥97.0%, CH_4 selectivity ≥99.7%). In the case of the RWGS reaction with the Cu/ZnO/Al_2O_3 catalyst, the CO_2 conversion monotonically increased from 2.0% to 78.1% with the temperature over the range of 100–650 °C (Fig. 3b). Compared with equilibrium conversion, the difference of CO_2 conversion was almost zero at 650 °C. Further increasing the

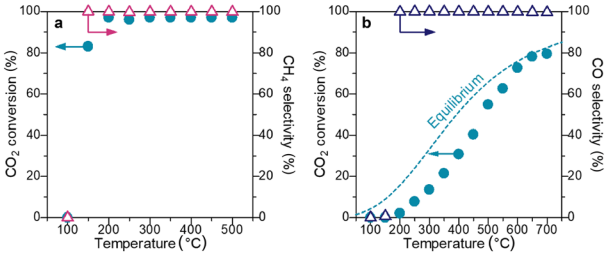

Fig. 3 (a) CO_2 conversion and CH_4 selectivity with respect to reaction temperature with Ni/CeO_2 catalyst; (b) CO_2 conversion and CO selectivity with respect to reaction temperature with $Cu/ZnO/Al_2O_3$ catalyst. The dependence of the amount of $Cu/ZnO/Al_2O_3$ is shown in Fig. S6.†

temperature to 700 °C did not significantly improve CO_2 conversion (79.4%). CO selectivity was high (≥99.3%) at a temperature of >200 °C.

2.2 Continuous production of O_2-free CO_2 from CO_2 + O_2 mixture

Prior to the continuous CO_2 capture and hydrogenation using the coupled tandem TSA/catalyst system, we demonstrated the continuous production of O_2-free CO_2 from a model combustion exhaust gas (10% CO_2 + 10% O_2/He) using the TSA system. Fig. 4a shows a schematic of the TSA system for O_2-free CO_2 production from the model combustion exhaust gas. Two reactors containing equal amounts of Rb-beta were set up in parallel for CO_2 capture and desorption. The CO_2 concentrations in effluents 1 and 2 were monitored by performing FTIR spectroscopy, and the O_2 concentration in effluent 1 was monitored by using mass spectrometry (MS). A gas mixture of CO_2 + O_2/He was fed into one reactor for 29.5 min for CO_2 capture and then purged with He (0.5 min) to remove the remaining O_2 from the reactor. The other reactor (containing CO_2-captured Rb-beta) was heated to 200 °C under He to produce O_2-free CO_2 in effluent 2. The details of this procedure are presented in Fig. S7.† Fig. 4b and d show the typical variations in the CO_2 and O_2 concentrations in effluents 1 and 2 over time, respectively. CO_2 is captured from the CO_2/O_2 mixture when the reactor is cooled from 200 to 40 °C. During the CO_2-capture period, the outlet CO_2 concentration (in effluent 1) is below the detection limit, indicating that CO_2 is almost completely removed from the 10% CO_2 + 10% O_2 mixture. Subsequently, two 4-way valves connected to the top and bottom of the tubular reactors are simultaneously switched, and the captured CO_2 is released by heating to 200 °C (5.5 °C min^{-1}) under He flow; this results in the formation of O_2-free CO_2 in effluent 2. The maximum concentration of the liberated CO_2 is ~37%. The amounts of captured CO_2 (12.1 mmol) and produced O_2-free CO_2 (11.9 mmol) in one cycle, calculated by applying eqn (2) and (3) in ESI† Text S3, are shown in Fig. S10 and S11. Note that the production of CO_2 results in an increase in the total flow rate (from 120 to 167 mL min^{-1}) of effluent 2. The CO_2 capture and desorption experiments are performed continuously for

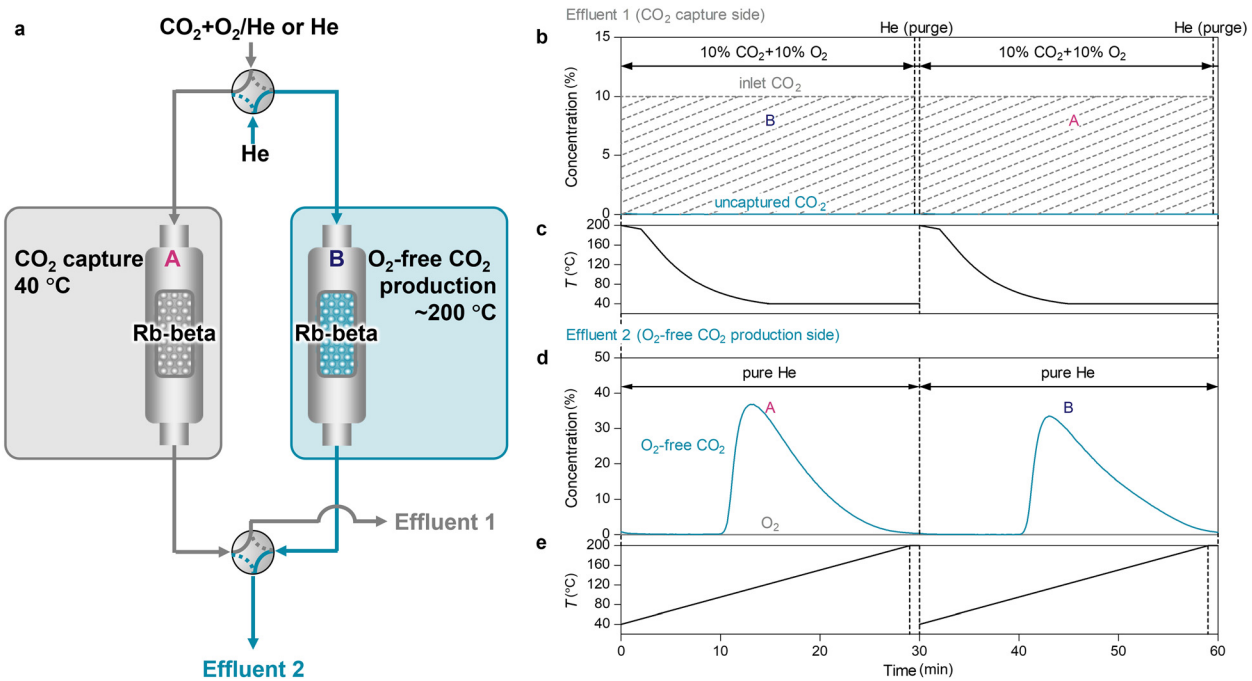

Fig. 4 (a) Schematic of the two-reactor TSA system for continuous CO_2 capture and O_2-free CO_2 production; captured gas (100 mL min^{-1}, 10% CO_2 + 10% O_2/He for 29.5 min and then pure He for 0.5 min) and released gas (120 mL min^{-1}, pure He for 30 min) were alternately fed into each reactor containing 14 g of Rb-beta; (b) and (d) typical variations in the CO_2 and O_2 concentrations in effluents 1 and 2 over time, respectively; (c) and (e) typical temperature changes in reactor A and B over time, respectively. O_2 concentration in effluent 1 is shown in Fig. S8.† The response curves for the outlet CO_2 over the blank are displayed in Fig. S9.†

seven cycles (Fig. S12†). These results clearly reveal the continuous production of O_2-free CO_2 from the 10% CO_2/10% O_2 gas mixture.

2.3 Continuous CO_2 capture and methanation/RWGS reaction using the tandem system

Next, continuous CO_2 capture and methanation were performed using the tandem TSA/methanation system. Unlike DFM designs, the tandem-system design allows individually optimized active sites and reaction conditions for each step. The proposed TSA system converts the model combustion exhaust (10% CO_2 + 10% O_2) to O_2-free CO_2, which undergoes methanation under H_2 in the reactor (containing Ni/CeO_2) downstream at 300 °C (Fig. 5a). Note that H_2 is expected to act as an inert gas, similar to He, because the Rb-beta sorbent does not promote hydrogenation. First, the CO_2 + O_2 mixture is fed into one reactor of the TSA system for 29.5 min for CO_2 capture, and then, pure He (0.5 min) is fed to purge the remaining O_2 in the reactor. The other reactor (containing CO_2-captured Rb-beta) is heated to 200 °C (5.5 °C min^{-1}) under pure H_2 for 30 min. The desorbed CO_2 and H_2 are fed into the methanation reactor and converted to CH_4. The details of this procedure are displayed in Fig. S13.†

Fig. 5b and d show the typical variations in the CH_4, CO_2, and O_2 concentrations in effluents 1 and 2 over time, analyzed online by employing an IR gas-cell and MS, respectively. Fig. 5c and e depict the optimized time variations in the temperatures of the two TSA reactors. During the CO_2-capture period, the outlet CO_2 concentration (in effluent 1) is below the detection limit, indicating that CO_2 is almost completely removed from the 10% CO_2 + 10% O_2 mixture. Subsequently, two 4-way valves connected to the top and bottom of the tubular reactors are simultaneously switched, and the captured CO_2 is released by heating under H_2. When CO_2-captured Rb-beta is heated under H_2, CH_4 was observed in effluent 2, with a maximum concentration of ~66.3%. The concentration of CO (0.02%) is low, and CO_2 is not present in effluent 2; thus, CH_4 selectivity is ≥99%. Note that the high conversion level of CO_2 and H_2 over the downstream Ni/CeO_2 catalyst results in a significant decrease in the total flow rate (from 120 to 40 mL min^{-1}) of effluent 2 (details on the decrease in the total flow rate are shown in ESI† Text S4 and Fig. S14 and S15). The CO_2 capture and desorption/methanation experiments are performed continuously for four cycles (Fig. S16†). Fig. S17 and S18† show the results of condition optimization for the CO_2 capture and desorption/methanation experiments. The effect of the CO_2-capture temperature (40, 80, 100, and 120 °C) on the CH_4 yield (Fig. S17†) reveals that the lowest temperature (40 °C) produces the highest CH_4 yield, simply because a lower adsorption temperature leads to a larger CO_2 capacity of Rb-beta. The effect of the catalyst amount (Fig. S18†) shows that increasing the catalyst amount (from 2 to 15 g) results in a slight increase in the CH_4 yield (from 85 to 92%) and a large decrease in the space–time-yield of CH_4 (STY_{CH_4}) (from 11.9 to 1.8 mmol g^{-1} h^{-1}).

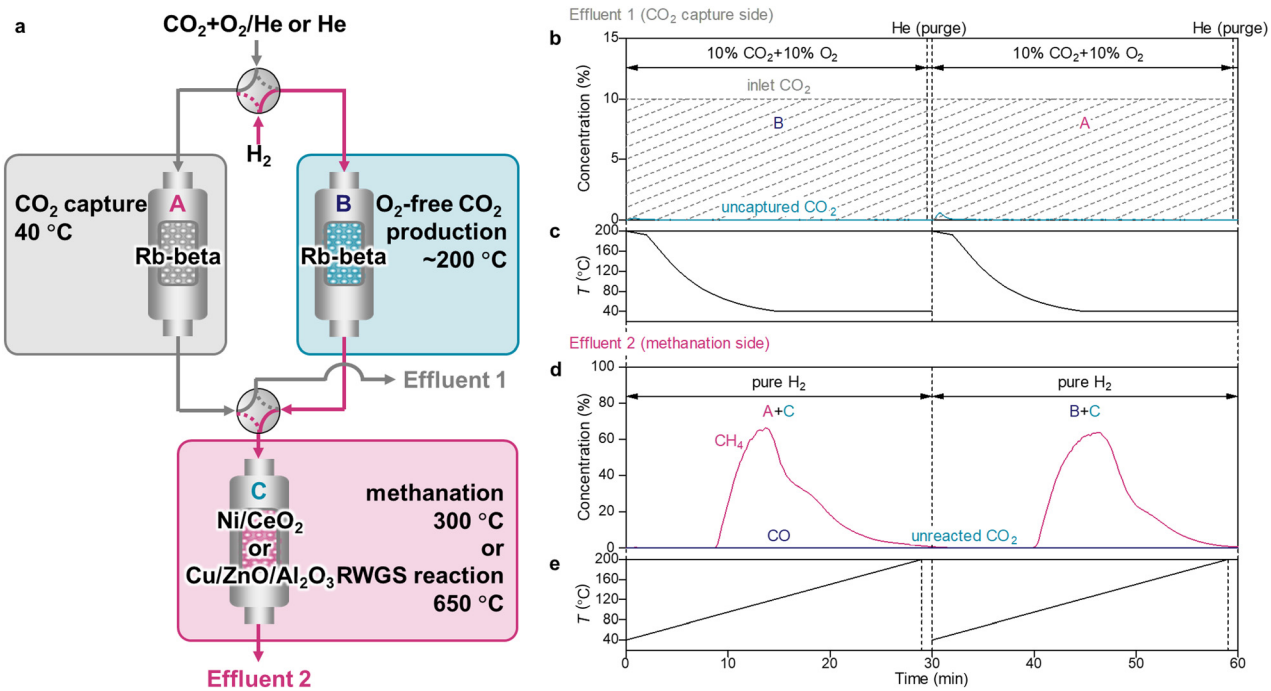

Fig. 5 (a) Schematic of the two-reactor TSA system for continuous CO_2 capture and methanation; captured gas (100 mL min^{-1}; 10% CO_2 + 10% O_2/He for 29.5 min and then pure He for 0.5 min) and hydrogenation gas (120 mL min^{-1}; pure H_2 for 30 min) were alternately fed into each reactor containing 14 g of Rb-beta; (b) and (d) typical variations in the CH_4, CO_2, and CO concentrations in effluents 1 and 2 over time, respectively; (c) and (e) typical temperature changes in reactor A and B over time, respectively.

A CH_4 yield of 92% is almost double those in the previously reported catalytic systems for the methanation of a CO_2/O_2 mixture using CCR (16 reports and 55 reaction processes presented in Fig. 6a; details are listed in Table S1†). The reaction temperature in our system (300 °C) is the lowest among the reported systems, and the inlet CO_2 concentration in our system is the highest among the reported systems. Note that the majority of the previously reported CCR systems for CH_4 production were tested in the absence of O_2 during the CO_2-capture period (10 reports and 100 reaction processes; details are listed in Table S2†). Compared with those systems, our system produces the highest CH_4 yield.

Under conditions relevant to future practical implementation, gas purging with unreacted gas is expected to be avoided, and recycling of unreacted H_2 is anticipated to be implemented. Continuous CO_2 capture and methanation were conducted using the tandem system without gas purging (Fig. S19†). Under these conditions, the effluent gas composition remained nearly unchanged compared to that observed under gas purge conditions (Fig. 5d), suggesting that the effect of transient O_2 inflow was negligible. This is possibly because oxidized Ni species were readily reduced during the initial introduction of H_2, demonstrating that this tandem system exhibits complete O_2-tolerance. While the current system shows high performance, future implementation of CH_4/H_2 product gas recycling as a reductive gas suggests the potential to further improve H_2 utilization efficiency.

We demonstrated continuous CO_2 capture and the RWGS reaction using a system similar to that described in the previous subsection; in this system, a commercial $Cu/ZnO/Al_2O_3$ catalyst was used as the RWGS catalyst (catalyst amount = 10 g) (Fig. S20†). When Rb-beta was heated from 40 to 200 °C, CO was formed with a maximum concentration of ~41.0%, CO_2 was desorbed with a maximum concentration of ~11.2%, and almost no CH_4 was detected (CO selectivity ≥99%). In addition, no CO_2 was detected in effluent 1 using gas-cell IR, indicating that almost all the supplied CO_2 was captured by Rb-beta. Given the CO production per unit time (a detailed explanation is presented in ESI† Text S5 and Fig. S21), the conversion of inlet CO_2 to CO (denoted as the CO yield) was 85%, indicating that a considerable amount of the supplied high-concentration CO_2 in the presence of O_2 was continuously converted to CO. This reaction was repeated several times and maintained for at least 2 h (six cycles; Fig. S22†). Furthermore, the amount of $Cu/ZnO/Al_2O_3$ included in this RWGS system was optimized from 0.2 to 14 g (Fig. S23†). When the catalyst amount was between 1 to 15 g, the CO yield was over 85% and the maximum CO production rate was 20.1 mmol g^{-1} h^{-1}. When the catalyst amount was decreased to 0.2 g, the CO yield decreased by 45% but the space–time-yield of CO (STY_{CO}) increased to 55.5 mmol g^{-1} h^{-1}. Thus, increasing the catalyst amount from 0.2 to 1 g resulted in a sharp increase in the CO yield (from 45% to 85%), but further increasing the amount from 1 to 15 g resulted in limited change (from 85% to 81%). Additionally, increasing the catalyst amount from 0.2 to 15 g significantly decreased the STY_{CO} from 55.5 to 1.5 mmol g^{-1} h^{-1}.

The system was compared with previously reported systems (10 reports and 30 reaction processes in Fig. 6b; details are listed in Table S3†). The majority of the previously reported CCR systems for CO production were evaluated at low inlet CO_2 concentrations (below 1%). Our system demonstrated the RWGS process with a high CO yield (85%) at a high inlet CO_2 concentration (10%). Notably, many of the previously studied CCR systems aimed at CO production were tested in the absence of O_2 during CO_2 capture (as detailed in Table S4;† 10 reports and 100 reaction processes). Compared with systems with the same inlet CO_2 concentration (10%), our system demonstrated approximately twice the CO yield.

For example, in Fischer–Tropsch (FT),[52] methanol (MeOH),[53] and ethanol (EtOH) syntheses[54] from syngas, the H_2/CO ratio of the syngas significantly affects the selectivity and yield of the product. Similar to the aforementioned methanation system, the H_2 input was optimized (Fig. 7). When the H_2 flow time was reduced from 30 to 20 min in one cycle, the H_2 conversion slightly increased from 9.8% to 15% and the H_2/CO ratio changed from 9.1 to 3.7, which is closer to the ideal value of 2.0 for FT, MeOH, and EtOH syntheses, while retaining a high CO yield (93%) (see ESI† Text S5 for details). Furthermore, syngas is an environment-friendly alternative gaseous fuel for internal combustion during engine operations, and H_2-rich syngas ($H_2/CO \geq 3.0$) has been reported to improve thermal efficiency;[55] this continuous RWGS process also has the potential to provide industrially valuable syngas. This technique is effective for continuous CO_2 capture and methanation. A decrease in the H_2 flow time improved the H_2 utilization efficiency (H_2 conversion increased from 38% to 58%; Fig. S24; see ESI† Text S6 for details).

In this chapter, we demonstrated that the developed tandem system is effective for the ambient-pressure conversion of CO_2 in model combustion exhaust into CH_4 and CO *via* methanation and RWGS reaction. Because this system does not require a pressure swing adsorption (PSA) unit, it has the potential to operate all reactors under

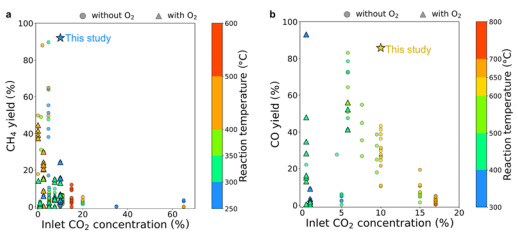

Fig. 6 Performance of (a) methanation and (b) RWGS reaction processes in the proposed system and previously reported systems for exhaust or atmospheric CO_2 conversion (references are listed in Tables S1–S4†).

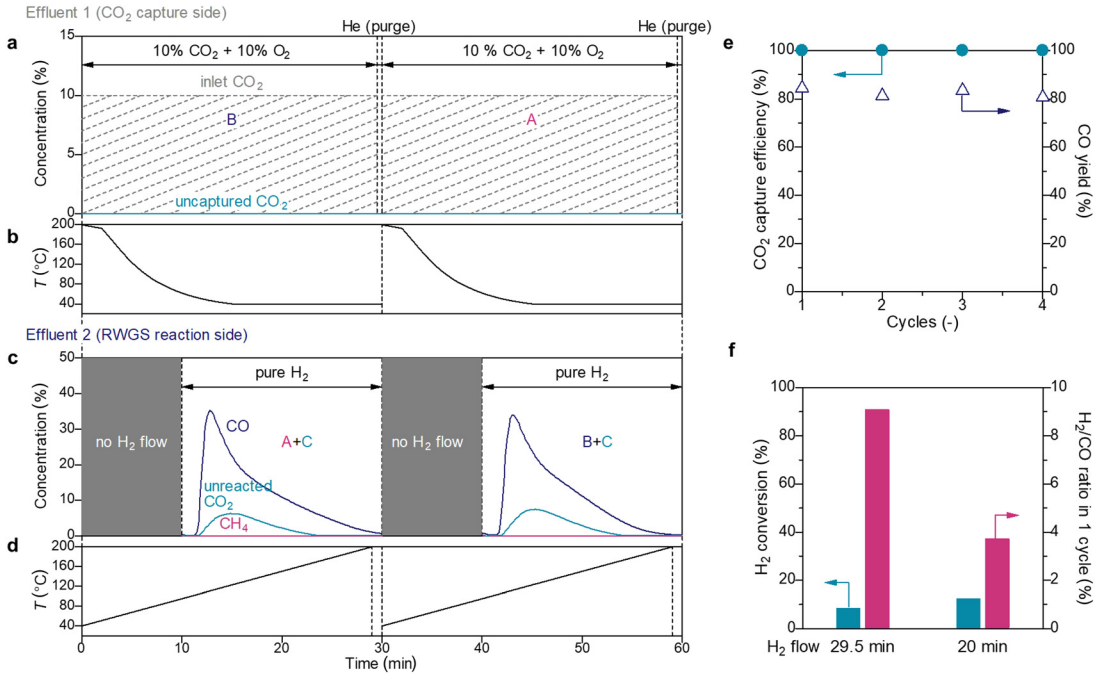

Fig. 7 Continuous CO_2 capture and methanation; captured gas (100 mL min^{-1}; 10% CO_2 + 10% O_2/He for 29.5 min and then pure He for 0.5 min) and hydrogenation gas (120 mL min^{-1}; pure H_2 for 20 min) were alternately fed into each reactor containing 14 g of Rb-beta. (a) and (c) typical variations in the CH_4, CO_2, and CO concentrations in effluents 1 and 2 over time, respectively; (b) and (d) typical temperature changes in reactors a and b over time, respectively; (e) changes in the CO_2 capture efficiency and CO yield during cyclic test; (f) comparison of H_2 conversion and ratio of effluent CO to H_2 in one cycle between the conditions depicted in Fig. S20a† (H_2 flow for 29.5 min) and those in Fig. 7a (H_2 flow for 20 min).

uniform pressurized conditions. This tandem system with conventional MeOH or FT synthesis catalysts such as $Cu/ZnO/Al_2O_3$ [56–58] and Fe-based catalysts,[59,60] which operate under elevated pressure, could enable the direct synthesis of methanol and liquefied petroleum gas (LPG) from CO_2 in model combustion exhaust streams.

2.4 Continuous direct air capture and methanation

Next, we broadened the applicability of the proposed system for continuous CH_4 production from ambient CO_2 (Fig. 8). For ambient CO_2 capture and methanation, a high flow rate (500 mL min^{-1}) of air was fed into one TSA reactor for 60 min, whereas a low flow rate (10 mL min^{-1}) of pure H_2 was fed to the other TSA reactor (containing CO_2-captured Rb-beta) for 60 min. The H_2 and desorbed CO_2 from the other TSA reactor were subsequently fed into the downstream methanation reactor (containing Ni/CeO_2). When CO_2-captured Rb-beta was heated under H_2, the desorbed CO_2 underwent methanation on the downstream Ni/CeO_2 catalyst to produce a high concentration of CH_4. The maximum CH_4 concentration was 0.7%, and the average CH_4 concentration

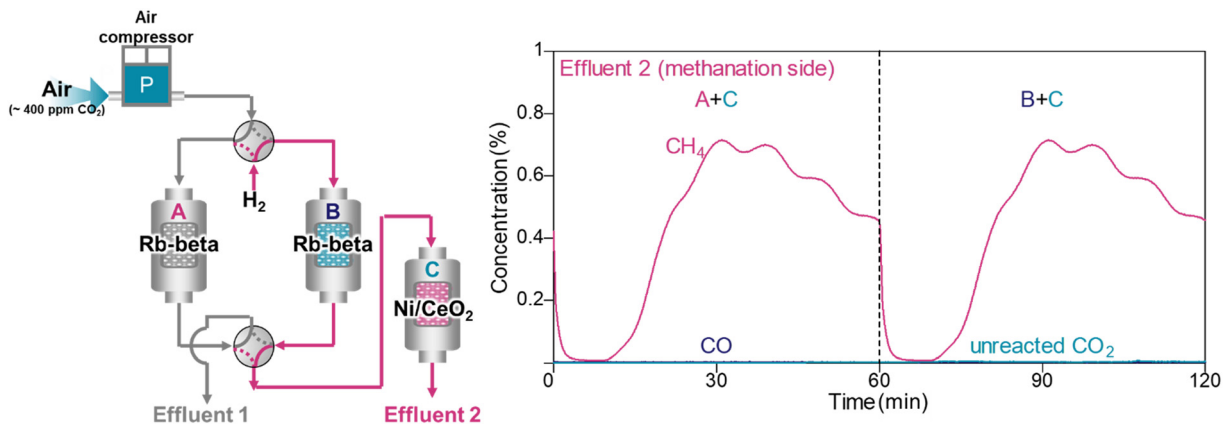

Fig. 8 Schematic and typical variations in the CH_4, CO, and unreacted CO_2 amounts in effluent 2 over time for continuous direct air capture and methanation. Conditions: 14 g of Rb-beta for each upper reactor and temperature swing from 40 to 200 °C (heating rate = 20 °C min^{-1}); 15 g of Ni/CeO_2 for the bottom reactor, 300 °C, and 500 mL min^{-1} air for 60 min and switched to 10 mL min^{-1} H_2 for another 60 min.

was ~0.4%. The results highlight the production of 10 times enriched CH_4 from atmospheric CO_2. As shown in our previous study,[61] the enrichment methodology is simply based on the difference in the flow rates for CO_2 capture (500 mL min^{-1}) and reduction (10 mL min^{-1}). As shown in Fig. S25,† the proposed methanation method is also applicable to high concentrations (40%) of CO_2. The 40% CO_2 + 10% O_2 mixture undergoes methanation, and the CH_4 yield is ~70%. These results demonstrate that the proposed methanation system can be applied to a wide range of CO_2 concentrations.

2.5 Energy efficiency

To assess the energy requirements of the two processes, we analyzed the energy efficiency (η) and fuel production efficiency (FPE) of the tandem methanation and CCR systems.[62] The η for CO_2 conversion reactions was calculated using the following equation:[63]

$$\eta\,(\%) = \frac{\Delta H_R\,(\mathrm{kJ\ mol^{-1}}) \cdot X_{CO_2} \cdot r_{CO_{2,in}}\,(\mathrm{mol\ s^{-1}})}{P\,(\mathrm{kW})},$$

where $r_{CO_{2,in}}$ represents the molar flow rate of CO_2 at the inlet of the reactor, and ΔH_R is the reaction enthalpy (−165 kJ mol^{-1} for the methanation process at 298 K). The calculated η values for the two systems are plotted as a function of time elapsed in Fig. 9a. The η for CCR is 46% at the beginning of the reaction but declines exponentially owing to the limited CO_2 capacity of the DFM. In contrast, the η for tandem methanation is significantly higher than that for CCR, owing to the lower total thermal input and greater CH_4 production. The system performances are compared in Fig. 9b. The advantages of tandem methanation over CCR are evident in terms of the CH_4 yield, CH_4 selectivity, CH_4 production per gram of the catalyst + adsorbent (to ensure a fair comparison between the two systems), and η. Note that the η for tandem methanation exceeds 100%. This is because only the power input is considered in the overall energy input and output and the net energy flow of the reactants and products is ignored.

We also compared the FPEs of the two systems. The FPE for the methanation reaction is defined as the ratio of the energy output in the form of methane (not considering unreacted H_2 at the exit) to the total energy input. The output energy is estimated based solely on the low heating value of CH_4 (LHV_{CH_4}), because the condensation heat of the produced water is typically not recovered. The energy input includes both the thermal input and the feed gas (H_2), which possesses a heating value and contributes energy to the process. Therefore, the FPE is calculated as

$$\mathrm{FPE}\ (\%) = \frac{\text{Output energy}}{\text{Input energy}} = \frac{\mathrm{LHV_{CH_4}\,(kJ\ mol^{-1})} \cdot r_{CH_4}\,(\mathrm{mol\ s^{-1}})}{P\,(\mathrm{kW}) + \mathrm{LHV_{H_2}\,(kJ\ mol^{-1})} \times (r_{H_2,in} - r_{H_2,out})\,(\mathrm{mol\ s^{-1}})}$$

where P is the thermal input, r_{CH_4} is the mole of CH_4 production, $r_{H_2,in} - r_{H_2,out} = (n_{H_2,in} - n_{H_2,out})/\Delta t$ is the rate of H_2 consumption, and LHV_{H_2} and LHV_{CH_4} are the LHVs of the converted hydrogen and methane (242 and 801 kJ mol^{-1}), respectively. As depicted in Fig. 9b, tandem methanation yields a high FPE of 83%, whereas CCR exhibits an FPE of 80%.

3 Conclusions

In summary, we developed a new method for the continuous production of O_2-free CO_2, CH_4, and CO from the atmosphere and a simulated exhaust gas (CO_2/O_2/He mixture). The

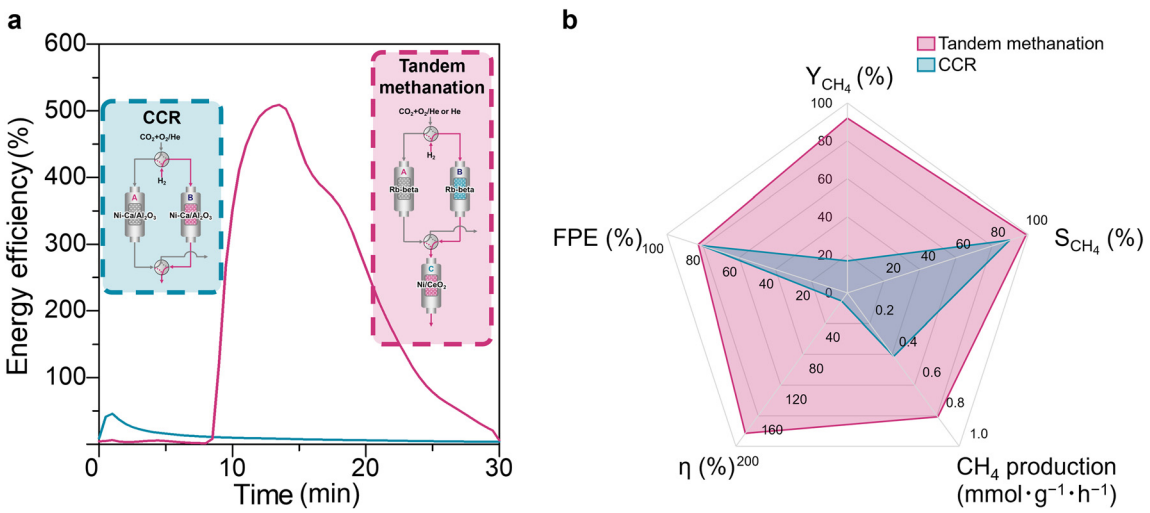

Fig. 9 (a) Typical variations in the energy efficiencies of CCR and tandem methanation system over time. Conditions: 14 g of Rb-beta for each upper reactor and temperature swing from 40 to 200 °C (heating rate = 20 °C min^{-1}); 15 g of Ni/CeO_2 for the bottom reactor, 300 °C, and 500 mL min^{-1} air for 60 min and switched to 10 mL min^{-1} H_2 for another 60 min; (b) comparison of the CH_4 yield (Y_{CH_4}), CH_4 selectivity (S_{CH_4}), CH_4 production, energy efficiency (η), and fuel production efficiency (FPE) between the CCR and tandem methanation system. Parameters explaining energy efficiency, such as η and FPE, are detailed in ESI† Text S7.

developed process is suitable for continuous operation over a low-temperature swing of 40–200 °C on a Rb-beta sorbent combined with a methanation system at 300 °C and a RWGS system (for syngas synthesis) at 650 °C. The results of this study revealed that the developed process is almost twice as effective as CCR for CO_2 capture and hydrogenation. We also provided evidence that the energy efficiency of the tandem methanation process based on the overall energy input and output is comparatively high because of the low power input required to operate the system and the high CH_4 production. This approach is promising for CO_2 utilization *via* direct air and post-combustion gas capture and conversion to green fuels. In the future, we expect that our flexible process, in combination with efficient catalysts, will contribute to a carbon-neutral society.

4 Methods

4.1 Sorbent and catalyst preparation

Beta (Si/Al = 5, Mitsui Mining & Smelting Co., Ltd.), 13X (Si/Al = 1.25, Junsei Chemical Co., Ltd.), and Na-Y zeolites (Si/Al = 2.75, JRC-Z-Y5.5, Tosoh Corporation) were used as sorbents and supports. To prepare Rb-loaded zeolite sorbents, Rb species were immobilized on the zeolites using the conventional impregnation method. An appropriate amount of a Rb_2CO_3 aqueous solution (AR > 99%, FUJIFILM WAKO Pure Chemical Corporation) was incorporated into the zeolites. After being stirred for 3 h at 25 °C, the suspension was evaporated by using a vacuum pump at 50 °C and dried overnight at 100 °C. The solid produced was then calcined at 200 °C for 1 h to obtain the desired Rb-zeolites. Other alkali-metal-loaded zeolite sorbents were prepared by employing the same approach using K_2CO_3 (AR: 99.0%, Tokyo Chemical Industry Co., Ltd.) and Cs_2CO_3 (AR > 99%, FUJIFILM WAKO Pure Chemical Corporation) as precursors.

4.2 Characterization

CO_2 adsorption measurements were performed by using a fixed-bed flow reactor (Fig. S1†). The zeolite sorbents (50 mg) were placed on quartz wool in the middle of a reactor, which was then placed in an electric tube furnace. The zeolite sorbents were heated to 500 °C under pure He flow (100 mL min^{-1}), maintained for 30 min to remove the CO_2 and water vapor included in the zeolites, and cooled to 40 °C. The gas emitted from the reactor outlet was directly connected to a homemade IR gas cell to monitor the CO_2 concentration by performing IR measurements. In the first 30 s, before the CO_2 concentration stabilized, a flow of 1% CO_2/He was passed through the bypass line and then the feed was switched to the reactor. The CO_2 adsorption amount was calculated from the difference in CO_2 concentrations between the blank and zeolites. Due to the high absorbance of CO_2 in gas-cell IR measurements, fluctuations in the ambient CO_2 concentration can lead to slight variations in the measured values. To evaluate the reproducibility, each sample was measured three times. The resulting deviation in CO_2 concentration was within approximately ±0.05%, corresponding to an error margin of about ±0.04 mmol g_{sor}^{-1} in the calculated CO_2 adsorption amount. The TPD of CO_2 was also performed using the homemade IR gas cell. The zeolite (100 mg) was pretreated in He atmosphere at 500 °C for 30 min and then cooled to 50 °C. Next, the 1% CO_2/N_2 (100 mL min^{-1}) mixed gas was fed into the reactor for 30 min and then He was flowed for 15 min. The TPD profile was obtained by heating the sample from 30 to 200 °C at a rate of 20 °C min^{-1} under He flow. *Operando* FTIR measurements were performed during the TPD of CO_2 using a JASCO FT/IR-4600 spectrometer equipped with a mercury–cadmium–telluride detector and a flow-type quartz IR cell connected to a flow system (total flow rate = 100 mL min^{-1}; Fig. S2†). The effluent gas was simultaneously monitored by performing FTIR spectroscopy (JASCO FT/IR-4600) using a homemade gas cell. A sample pellet (40 mg; diameter: 20 mm) was introduced into a quartz cell equipped with a CaF window. The sample pellet was pretreated at 200 °C for 30 min under He flow and cooled to 40 °C, and the 1% CO_2/He mixture was fed into the reactor for 5 min. Subsequently, the system was purged with He for 10 min and the background spectrum was recorded. Temperature-resolved measurements were performed from 40 to 200 °C. The *operando* IR measurements were performed by monitoring the desorption of CO_2 in the outlet gas mixture.

4.3 Continuous CO_2 capture and O_2-free CO_2 production using two parallel reactors

Continuous CO_2 capture and O_2-free CO_2 production were performed using a system similar to that in a previous study.[61] CO_2 was continuously separated by using two fixed-bed flow reactors (Fig. S7†), and the response curves for CO_2 were obtained using a blank test (Fig. S9†). Two vertical quartz reactors (A and B) containing the same sorbent powder (14 g) were placed on quartz wool in the middle of the reactor in an electric tube furnace. The sorbents were pretreated under pure He flow (100 mL min^{-1}) at 400 °C. Subsequently, continuous CO_2 capture and O_2-free CO_2 production were achieved. Two timer-controlled 4-way valves were switched simultaneously to feed a simulated exhaust gas (100 mL min^{-1}; 10% CO_2 + 10% O_2/He for 29.5 min and He for 0.5 min) and an O_2-free CO_2 gas (120 mL min^{-1}; He for 30 min); when the simulated exhaust gas was fed to reactor A, the O_2-free CO_2 gas was fed to reactor B. Effluent gases containing uncaptured CO_2 from reactor A and B (with O_2 and He) were continuously fed into effluent 1. The produced O_2-free CO_2 in reactors A and B (with He) was continuously fed into effluent 2. The effluent gas was simultaneously monitored by performing FTIR spectroscopy (JASCO FT/IR-4600) using a gas cell and a mass spectrometer (BELMass, MicrotracBEL Corp.). The CO_2 concentration was calculated using the calibration curve for the CO_2 concentration and the IR peak area in the range of 2395–2235 cm^{-1} for ≤1% CO_2 and 3760–3662 cm^{-1} for >1% CO_2. The CO_2 capture efficiency and the yield of O_2-free CO_2 were calculated as follows:

$$\text{CO}_2\text{ capture efficiency [\%]} = \frac{\int_0^t \left[F^{\text{in}}_{\text{CO}_2} - F^{\text{out(1)}}_{\text{CO}_2}(t) \right] \text{d}t}{\int_0^t F^{\text{in}}_{\text{CO}_2}(t)\text{d}t} \times 100;$$

$$\text{Yield of O}_2\text{ free CO}_2\text{ [\%]} = \frac{\int_0^t F^{\text{out(2)}}_{\text{CO}_2}(t)\text{d}t}{\int_0^t F^{\text{in}}_{\text{CO}_2}(t)\text{d}t} \times 100,$$

where $F^{\text{in}}_{\text{CO}_2}$, $F^{\text{out(1)}}_{\text{CO}_2}$, and $F^{\text{out(2)}}_{\text{CO}_2}$ are the CO_2 molar flow rates at the column inlet and the outlets of effluents 1 and 2, respectively, and t denotes the duration of one cycle.

4.4 Continuous CO_2 capture and methanation/RWGS reaction using the combined system with two parallel reactors for TSA and a single reactor for hydrogenation

Continuous CO_2 capture and hydrogenation (such as the methanation and RWGS reactions) were performed using homemade reactors (Fig. 1c; detailed procedure is shown in Fig. S13†). Two vertical quartz reactors (A and B) containing the Rb-beta sorbent powder (14 g), same as those used for O_2-free CO_2 production, were placed on quartz wool in the middle of the reactor in an electric tube furnace. For the methanation and RWGS reactions, Ni/CeO_2 and $Cu/ZnO/Al_2O_3$ (commercial, Alfa Aesar) were added to the bottom reactor (C). The sorbents were pretreated under He flow for 30 min at 400 °C. Ni/CeO_2 was pretreated with H_2 for 30 min at 400 °C. $Cu/ZnO/Al_2O_3$ was pretreated with H_2 for 30 min at 500 °C. After these pretreatments, continuous CO_2 capture and hydrogenation were performed. Similar to the continuous O_2-free CO_2 production system, 1% CO_2 + 10% O_2/He or pure He (for purging) and pure H_2 were alternately flowed to each Rb-beta under cooling and heating. The produced O_2-free CO_2 and H_2 were fed into a hydrogenation catalyst (in reactor C). Effluent 1 contained the uncaptured CO_2, O_2, and He. Effluent 2 contained the produced CH_4, CO, and unreacted CO_2. The produced H_2O was trapped before the gas concentrations were analyzed using cold trap equipment. The gas compositions in effluents 1 and 2 (CO_2, CO, and CH_4) were analyzed online by using an FTIR spectrometer (JASCO FT/IR-4600) with a gas cell. The STY_{CH_4}, STY_{CO}, CH_4, and CO yields and H_2 conversion are calculated as follows:

$$\text{STY}_{\text{CH}_4}\text{ or STY}_{\text{CO}}\ \left[\text{mmol g}^{-1}\ \text{h}^{-1}\right] = \frac{\int_0^t F^{\text{out}}_{\text{CH}_4\text{ or CO}}(t)\text{d}t}{m_{\text{cat}} \times t};$$

$$\text{CH}_4\text{ or CO yield [\%]} = \frac{\int_0^t F^{\text{out}}_{\text{CH}_4\text{ or CO}}(t)\text{d}t}{\int_0^t F^{\text{in}}_{\text{CO}_2}(t)\text{d}t} \times 100,$$

$$\text{H}_2\text{ conversion [\%]} = \frac{\int_0^t F^{\text{out}}_{\text{CO}}(t)\text{d}t + 4\int_0^t F^{\text{out}}_{\text{CH}_4}(t)\text{d}t}{\int_0^t F^{\text{in}}_{\text{H}_2}(t)\text{d}t} \times 100$$

where $F^{\text{out}}_{\text{CH}_4}$ and $F^{\text{out}}_{\text{CO}}$ are the CH_4 and CO molar flow rates, respectively, at the column outlet of effluent 2, $F^{\text{in}}_{\text{CO}_2}$ and $F^{\text{in}}_{\text{H}_2}$ are the CO_2 and H_2 molar flow rates at the column inlet, and m_{cat} is the catalyst mass. H_2 conversion was calculated based on the stoichiometric consumption primarily associated with the formation of CO and CH_4. To determine the CO and CH_4 molar flow rates, the peak area values around 2250–2001 and 3031–2994 cm^{-1} were used, respectively. The power consumption (P) for reactor heating, which represents the thermal input, was measured using an electrical power consumption analyser (ELPA, EC-05EB).

4.5 Continuous CCR to CH_4 system

Continuous CO_2 capture and reduction to CH_4 using the combined two parallel reactors were performed using homemade reactors (Fig. S1a†). Two vertical quartz reactors (A and B), each containing the $Ni–Ca/Al_2O_3$ sieves, were placed on quartz wool in the middle of an electric tube furnace. Each $Ni–Ca/Al_2O_3$ was pretreated with H_2 for 30 min at 500 °C. After these pretreatments, continuous CCR was performed. 1% CO_2 + 10% O_2/He and pure H_2 were alternately flowed to each $Ni–Ca/Al_2O_3$ under isothermal conditions. Effluent 1 contained the uncaptured CO_2, O_2, and He. Effluent 2 contained the produced CH_4, CO, and unreacted CO_2. The produced H_2O was trapped before the gas concentrations were analyzed using cold trap equipment. The gas compositions in effluents 1 and 2 (CO_2, CO, and CH_4) were analyzed online by using an FTIR spectrometer (JASCO FT/IR-4600) with a gas cell.

Data availability

The data that support the findings of this study are available from the corresponding author upon reasonable request.

Author contributions

S. Miy. wrote the manuscript draft and conducted the majority of the experiments, including validation and methodology development (writing – original draft, investigation, validation, methodology). A. A. supervised the project and contributed to manuscript revision (supervision, writing – review & editing). Y. M. and H. S. F. assisted with catalyst preparation and performed catalytic activity trials (investigation, validation). S. Min. and T. T. provided valuable insights into the experimental work and contributed to data visualization and manuscript revision (visualization, writing – review & editing). K. S. designed and supervised the overall project and secured funding (supervision, conceptualization, writing – review & editing, funding acquisition).

Conflicts of interest

There are no conflicts to declare.

Acknowledgements

This study was supported by the "Moonshot Research and Development Program" (JPNP18016), commissioned by the New Energy and Industrial Technology Development Organization (NEDO), KAKENHI (23K20034,

and 21H04626) from the Japan Society for the Promotion of Science (JSPS) and the Joint Usage/Research Center for Catalysis. S. Miy. acknowledges the Grant-in-Aid for JSPS Fellows (24KJ0267, DC2).

References

1 D. A. Lashof and D. R. Ahuja, Relative contributions of greenhouse gas emissions to global warming, *Nature*, 1990, **344**, 529–531.
2 E. S. Sanz-Pérez, C. R. Murdock, S. A. Didas and C. W. Jones, Direct capture of CO_2 from ambient air, *Chem. Rev.*, 2016, **116**, 11840–11876.
3 C. F. Schleussner, J. Rogelj, M. Schaeffer, T. Lissner, R. Licker, E. M. Fischer, R. Knutti, A. Levermann, K. Frieler and W. Hare, Science and policy characteristics of the Paris Agreement temperature goal, *Nat. Clim. Change*, 2016, **6**, 827–835.
4 S. Fawzy, A. I. Osman, J. Doran and D. W. Rooney, Strategies for mitigation of climate change: A review, *Environ. Chem. Lett.*, 2020, **18**, 2069–2094.
5 M. Tamura, M. Honda, Y. Nakagawa and K. Tomishige, Direct conversion of CO_2 with diols, aminoalcohols and diamines to cyclic carbonates, cyclic carbamates and cyclic ureas using heterogeneous catalysts, *J. Chem. Technol. Biotechnol.*, 2014, **89**, 19–33.
6 A. Álvarez, A. Bansode, A. Urakawa, A. V. Bavykina, T. A. Wezendonk, M. Makkee, J. Gascon and F. Kapteijn, Challenges in the greener production of formates/formic acid, methanol, and DME by heterogeneously catalyzed CO_2 hydrogenation processes, *Chem. Rev.*, 2017, **117**, 9804–9838.
7 International Energy Agency, *The Future of Hydrogen: Seizing Today's Opportunities*, IEA, Paris, 2019.
8 C. Gough, Carbon capture and storage: A review of the global status, *Int. J. Greenhouse Gas Control*, 2008, **2**, 155–168.
9 S. Kammerer, I. Borho, J. Jung and M. S. Schmidt, Review: CO_2 capturing methods of the last two decades, *Int. J. Environ. Sci. Technol.*, 2023, **20**, 8087–8104.
10 H. A. Patel, J. Byun and C. T. Yavuz, Carbon dioxide capture adsorbents: Chemistry and methods, *ChemSusChem*, 2017, **10**, 1303–1317.
11 I. S. Omodolor, H. O. Otor, J. A. Andonegui, B. J. Allen and A. C. Alba-Rubio, Dual-function materials for CO_2 capture and conversion: A review, *Ind. Eng. Chem. Res.*, 2020, **59**, 17612–17631.
12 B. Shao, Y. Zhang, Z. Sun, J. Li, Z. Gao, Z. Xie, J. Hu and H. Liu, CO_2 capture and in-situ conversion: recent progresses and perspectives, *Green Chem. Eng.*, 2022, **3**, 189–198.
13 L. F. Bobadilla, J. M. Riesco-García, G. Penelás-Pérez and A. Urakawa, Enabling continuous capture and catalytic conversion of flue gas CO_2 to syngas in one process, *J. CO2 Util.*, 2016, **14**, 106–111.
14 M. S. Duyar, M. A. A. Treviño and R. J. Farrauto, Dual function materials for CO_2 capture and conversion using renewable H_2, *Appl. Catal., B*, 2015, **168–169**, 370–376.
15 F. Kosaka, Y. Liu, S. Y. Chen, T. Mochizuki, H. Takagi, A. Urakawa and K. Kuramoto, Enhanced activity of integrated CO_2 capture and reduction to CH_4 under pressurized conditions toward atmospheric CO_2 utilization, *ACS Sustainable Chem. Eng.*, 2021, **9**, 3452–3463.
16 M. Sakai, H. Imagawa and N. Baba, Layered-double-hydroxide-based Ni catalyst for CO_2 capture and methanation, *Appl. Catal., A*, 2022, **647**, 118904.
17 L. Li, S. Miyazaki, Z. Wu, T. Toyao, R. Selyanchyn, Z. Maeno, S. Fujikawa and K. Shimizu, Continuous direct air capture and methanation using combined system of membrane-based CO_2 capture and Ni-Ca based dual functional materials, *Appl. Catal., B*, 2023, **339**, 123151.
18 L. Li, Z. Wu, S. Miyazaki, T. Toyao, Z. Maeno and K. Shimizu, Continuous CO_2 capture and methanation over Ni–Ca/Al_2O_3 dual functional materials, *RSC Adv.*, 2023, **13**, 2213–2219.
19 S. Miyazaki, L. Li, S. Yasumura, K. W. Ting, T. Toyao, Z. Maeno and K. Shimizu, Continuous CO_2 capture and selective hydrogenation to CO over Na-promoted Pt nanoparticles on Al_2O_3, *ACS Catal.*, 2022, **12**, 2639–2650.
20 L. Li, N. Zhang, Z. Wu, S. Miyazaki, T. Toyao, Z. Maeno and K. Shimizu, Rb-Ni/Al_2O_3 as dual functional material for continuous CO_2 capture and selective hydrogenation to CO, *Chem. Eng. J.*, 2023, **477**, 147199.
21 B. Lu, Y. Fan, X. Zhi, Z. Han, F. Wu, X. Li, C. Luo and L. Zhang, Material design and prospect of dual-functional materials for integrated carbon dioxide capture and conversion, *Carbon Capture Sci. Technol.*, 2024, **12**, 100207.
22 M. T. Dunstan, F. Donat, A. H. Bork, C. P. Grey and C. R. Müller, CO_2 Capture at medium to high temperature using solid oxide-based sorbents: fundamental aspects, mechanistic insights, and recent advances, *Chem. Rev.*, 2021, **121**, 12681–12745.
23 K. T. Leperi, D. Yancy-Caballero, R. Q. Snurr and F. You, 110th anniversary: Surrogate models based on artificial neural networks to simulate and optimize pressure swing adsorption cycles for CO_2 capture, *Ind. Eng. Chem. Res.*, 2019, **58**, 18241–18252.
24 M. Krödel, A. Landuyt, P. M. Abdala and C. R. Müller, Mechanistic understanding of CaO-based sorbents for high-temperature CO_2 capture: Advanced characterization and prospects, *ChemSusChem*, 2020, **13**, 6259–6272.
25 S. Miyazaki, D. Chen, B. Jiacheng, T. Toyao, Y. Kanda and K. Shimizu, *In situ* spectroscopic study of CO_2 capture and methanation over Ni–Ca based dual functional materials, *Chem. – Asian J.*, 2024, **19**, e202301003.
26 Z. Tao, Y. Tian, W. Wu, Z. Liu, W. Fu, C.-W. Kung and J. Shang, Development of zeolite adsorbents for CO_2 separation in achieving carbon neutrality, *npj Mater. Sustain.*, 2024, **2**, 20.
27 D. G. Boer, J. Langerak and P. P. Pescarmona, Zeolites as selective adsorbents for CO_2 separation, *ACS Appl. Energy Mater.*, 2023, **6**, 2634–2656.
28 G. Shah, E. Ahmad, K. K. Pant and V. K. Vijay, Comprehending the contemporary state of art in biogas

enrichment and CO_2 capture technologies via swing adsorption, *Int. J. Hydrogen Energy*, 2021, **46**, 6588–6612.
29 Q. Ma, J. Li, Y. Li and J. Choi, Recent progress and issues facing zeolite and metal-organic framework membranes: From membrane synthesis to applications, *J. Membr. Sci.*, 2024, **690**, 122201.
30 N. Rangnekar, N. Mittal, B. Elyassi, J. Caro and M. Tsapatsis, Zeolite membranes – a review and comparison with MOFs, *Chem. Soc. Rev.*, 2015, **44**, 7128–7154.
31 S. Tada, H. Nagase, N. Fujiwara and R. Kikuchi, What are the best active sites for CO_2 methanation over Ni/CeO_2?, *Energy Fuels*, 2021, **35**, 5241–5251.
32 G. Zhou, H. Liu, K. Cui, A. Jia, G. Hu, Z. Jiao, Y. Liu and X. Zhang, Role of surface Ni and Ce species of Ni/CeO_2 catalyst in CO_2 methanation, *Appl. Surf. Sci.*, 2016, **383**, 248–252.
33 L. Li, W. Zeng, M. Song, X. Wu, G. Li and C. Hu, Research progress and reaction mechanism of CO_2 methanation over Ni-Based catalysts at low temperature: A review, *Catalysts*, 2022, **12**, 244.
34 H. Zhou, S. R. Docherty, N. Phongprueksathat, Z. Chen, A. V. Bukhtiyarov, I. P. Prosvirin, O. V. Safonova, A. Urakawa, C. Copéret, C. R. Müller and A. Fedorov, Combining atomic layer deposition with surface organometallic chemistry to enhance atomic-scale interactions and improve the activity and selectivity of Cu–Zn/SiO_2 catalysts for the hydrogenation of CO_2 to methanol, *JACS Au*, 2023, **3**, 2536–2549.
35 M. Behrens, F. Studt, I. Kasatkin, S. Kühl, M. Hävecker, F. Abild-Pedersen, S. Zander, F. Girgsdies, P. Kurr, B.-L. Kniep, M. Tovar, R. W. Fischer, J. K. Nørskov and R. Schlögl, The active site of methanol synthesis over Cu/ZnO/Al_2O_3 industrial catalysts, *Science*, 2012, **336**, 893–897.
36 T. Lunkenbein, J. Schumann, M. Behrens, R. Schlögl and M. G. Willinger, Formation of a ZnO overlayer in industrial Cu/ZnO/Al_2O_3 catalysts induced by strong metal–support interactions, *Angew. Chem., Int. Ed.*, 2015, **54**, 4544–4548.
37 S. Miyazaki, Z. Li, Z. Maeno, T. Toyao, M. Ito, Y. Nakajima and K. Shimizu, *Operando* Ce K-edge XANES study of low-loading Ni/CeO_2 in chemical looping dry reforming of methane, *Chem. Lett.*, 2022, **51**, 914–918.
38 N. Rui, X. Zhang, F. Zhang, Z. Liu, X. Cao, Z. Xie, R. Zou, S. D. Senanayake, Y. Yang, J. A. Rodriguez and C.-J. Liu, Highly active Ni/CeO_2 catalyst for CO_2 methanation: Preparation and characterization, *Appl. Catal., B*, 2021, **282**, 119581.
39 R.-P. Ye, Q. Li, W. Gong, T. Wang, J. J. Razink, L. Lin, Y.-Y. Qin, Z. Zhou, H. Adidharma, J. Tang, A. G. Russell, M. Fan and Y.-G. Yao, High-performance of nanostructured Ni/CeO_2 catalyst on CO_2 methanation, *Appl. Catal., B*, 2020, **268**, 118474.
40 Y. Han, M. Tian, C. Wang, Y. Kang, L. Kang, Y. Su, C. Huang, T. Zong, J. Lin, B. Hou, X. Pan and X. Wang, Highly active and anticoke Ni/CeO_2 with ultralow Ni loading in chemical looping dry reforming via the strong metal–support interaction, *ACS Sustainable Chem. Eng.*, 2021, **9**, 17276–17288.
41 J. Sun, S. Wan, F. Wang, J. Lin and Y. Wang, Selective synthesis of methanol and higher alcohols over Cs/Cu/ZnO/Al_2O_3 catalysts, *Ind. Eng. Chem. Res.*, 2015, **54**, 7841–7851.
42 Y. Zhang, Q. Sun, J. Deng, D. Wu and S. Chen, A high activity Cu/ZnO/Al_2O_3 catalyst for methanol synthesis: Preparation and catalytic properties, *Appl. Catal., A*, 1997, **158**, 105–120.
43 Q. Wang, Z. Yu, J. Feng, P. Fornasiero, Y. He and D. Li, Insight into the effect of dual active Cu^0/Cu^+ sites in a Cu/ZnO-Al_2O_3 catalyst on 5-hydroxylmethylfurfural hydrodeoxygenation, *ACS Sustainable Chem. Eng.*, 2020, **8**, 15288–15298.
44 H. Zhang, J. Chen, X. Han, Y. Pan, Z. Hao, S. Tang, X. Zi, Z. Zhang, P. Gao, M. Li, J. Lv and X. Ma, High-performance Cu/ZnO/Al_2O_3 catalysts for CO_2 hydrogenation to methanol, *Ind. Eng. Chem. Res.*, 2024, **63**, 6210–6221.
45 S. B. Waghmode, R. Vetrivel, S. G. Hegde, C. S. Gopinath and S. Sivasanker, Physicochemical investigations of the basicity of the cation exchanged ETS-10 molecular sieves, *J. Phys. Chem. B*, 2003, **107**, 8517–8523.
46 S. T. Yang, J. Kim and W. S. Ahn, CO_2 adsorption over ion-exchanged zeolite beta with alkali and alkaline earth metal ions, *Microporous Mesoporous Mater.*, 2010, **135**, 90–94.
47 K. S. Walton, M. B. Abney and M. D. LeVan, CO_2 adsorption in Y and X zeolites modified by alkali metal cation exchange, *Microporous Mesoporous Mater.*, 2006, **91**, 78–84.
48 R. Osuga, T. Yokoi and J. N. Kondo, Probing the basicity of lattice oxygen on H-form zeolites using CO_2, *J. Catal.*, 2019, **371**, 291–297.
49 J. C. Lavalley, Infrared spectrometric studies of the surface basicity of metal oxides and zeolites using adsorbed probe molecules, *Catal. Today*, 1996, **27**, 377–401.
50 G. Busca and V. Lorenzelli, Infrared spectroscopic identification of species arising from reactive adsorption of carbon oxides on metal oxide surfaces, *Mater. Chem.*, 1982, **7**, 89–126.
51 R. W. Stevens, R. V. Siriwardane and J. Logan, *In situ* Fourier transform infrared (FTIR) investigation of CO_2 adsorption onto zeolite materials, *Energy Fuels*, 2008, **22**, 3070–3079.
52 T. Riedel, M. Claeys, H. Schulz, G. Schaub, S.-S. Nam, K.-W. Jun, M.-J. Choi, G. Kishan and K.-W. Lee, Comparative study of Fischer–Tropsch synthesis with H_2/CO and H_2/CO_2 syngas using Fe- and Co-based catalysts, *Appl. Catal., A*, 1999, **186**, 201–213.
53 X. Yin, D. Y. C. Leung, J. Chang, J. Wang, Y. Fu and C. Wu, Characteristics of the synthesis of methanol using biomass-derived syngas, *Energy Fuels*, 2005, **19**, 305–310.
54 G. Liu, G. Yang, X. Peng, J. Wu and N. Tsubaki, Recent advances in the routes and catalysts for ethanol synthesis from syngas, *Chem. Soc. Rev.*, 2022, **51**, 5606–5659.
55 B. B. Sahoo, N. Sahoo and U. K. Saha, Effect of H_2: CO ratio in syngas on the performance of a dual fuel diesel engine operation, *Appl. Therm. Eng.*, 2012, **49**, 139–146.
56 A. Beck, M. A. Newton, L. G. A. van de Water and J. A. van Bokhoven, The enigma of methanol synthesis by Cu/ZnO/Al_2O_3-based catalysts, *Chem. Rev.*, 2024, **124**, 4543–4678.

57 G. Pacchioni, From CO_2 to methanol on $Cu/ZnO/Al_2O_3$ industrial catalyst. What do we know about the active phase and the reaction mechanism?, *ACS Catal.*, 2024, **14**, 2730–2745.
58 M. Behrens, F. Studt, I. Kasatkin, S. Kühl, M. Hävecker, F. Abild-Pedersen, S. Zander, F. Girgsdies, P. Kurr, B.-L. Kniep, M. Tovar, R. W. Fischer, J. K. Nørskov and R. Schlögl, The active site of methanol synthesis over $Cu/ZnO/Al_2O_3$ industrial catalysts, *Science*, 2012, **336**, 893–897.
59 L. Guo, J. Sun, Q. Ge and N. Tsubaki, Recent advances in direct catalytic hydrogenation of carbon dioxide to valuable C_{2+} hydrocarbons, *J. Mater. Chem. A*, 2018, **6**, 23244–23262.
60 W. Zhou, K. Cheng, J. Kang, C. Zhou, V. Subramanian, Q. Zhang and Y. Wang, New horizon in C1 chemistry: breaking the selectivity limitation in transformation of syngas and hydrogenation of CO_2 into hydrocarbon chemicals and fuels, *Chem. Soc. Rev.*, 2019, **48**, 3193–3228.
61 S. Miyazaki, M. Yoshihara, T. Toyao, Z. Maeno and K. Shimizu, Continuous production of O_2-free enriched CO_2 from ambient air using moisture swing sorbents, *N. Nanotechnol.*, 2023, **3–4**, 100029.
62 S. Ullah, Y. Gao, L. Dou, Y. Liu, T. Shao, Y. Yang and A. B. Murphy, Recent trends in plasma-assisted CO_2 methanation: A critical review of recent studies, *Plasma Chem. Plasma Process.*, 2023, **43**, 1335–1383.
63 R. Dębek, F. Azzolina-Jury, A. Travert and F. Maugé, A review on plasma-catalytic methanation of carbon dioxide – Looking for an efficient catalyst, *Renewable Sustainable Energy Rev.*, 2019, **116**, 109427.